

## Multi-modal Data Integration for Computer-Aided Ablation of Atrial Fibrillation

Jonghye Woo<sup>1</sup>, Byung-Woo Hong<sup>2</sup>, Sunil Kumar<sup>3</sup>, Indranill Basu Ray<sup>4</sup> and C.-C. Jay Kuo<sup>1</sup>

<sup>1</sup>Department of Electrical Engineering, University of Southern California, Los Angeles, CA 90089-2564

<sup>2</sup>Computer Science Department, University of California, Los Angeles, CA 90095

<sup>3</sup>Electrical and Computer Engineering Department, San Diego State University, San Diego, CA 92182

<sup>4</sup>School of Medicine and Dental Sciences, State University of New York at Buffalo, Buffalo, NY 14214

E-mails: jonghyew@usc.edu, hong@cs.ucla.edu, skumar@mail.sdsu.edu

indranillbasuray@yahoo.com, cckuo@sipi.usc.edu

Image-guided percutaneous interventions have successfully replaced invasive surgical methods in some cardiologic practice, where the use of 3D reconstructed cardiac images generated by Magnetic Resonance Imaging (MRI) and Computed Tomography (CT) plays an important role. To conduct computer-aided catheter ablation of atrial fibrillation accurately, multi-modal information integration with electroanatomic mapping (EAM) data and MRI/CT images is considered in this work. Specifically, we propose a variational formulation for surface reconstruction and incorporate the prior shape knowledge, which results in a level set method. The proposed method enables simultaneous reconstruction and registration under non-rigid deformation. Promising experimental results show the potential of the proposed approach.

### 1 INTRODUCTION

Current treatment of cardiac arrhythmias ranges from non-invasive strategies such as pharmacological therapy, to minimally invasive techniques such as catheter-based ablation, and to open surgical techniques. While medical therapy can mitigate the occurrence of arrhythmias, these treatments may have significant side effects since most drugs used have some toxicity that is not suitable for long-term therapy. The catheter-based procedure is proven to be an effective method in treating patients with certain cardiac arrhythmias [26]. It is much less invasive and more established. It also demands shorter recovery time than the surgical approach. Thus, catheter-based radio frequency (RF) ablation has become a widely accepted method in the treatment of cardiac arrhythmias, including Atrial Fibrillation (AF) and Ventricular Tachycardia (VT). These arrhythmias affect a large number of people and result in significant morbidity and mortality.

AF is the most common sustained cardiac arrhythmia encountered in clinical practice. In the United States alone, there are over 3.5 million patients with this disorder [17]. AF can result in serious complications, including congestive heart failure and thromboembolism. Despite recent advances, drug therapy to control this disease is still unsatisfactory. As an

alternative, a non-pharmacological, interventional approach based on creating percutaneous catheter-based lesion inside the heart has been developed. Lesions are delivered in the left atrial-pulmonary vein junction with an aim to electrically isolate these veins from the rest of the atrium. This protects the atrium from fast heart beating that is originated in the veins, which initiate and perpetuate AF.

The procedure of interventional AF treatment entails mapping the left atrium and the attached pulmonary veins using an electroanatomic mapping (EAM) system. This mapping information can be used to deliver lesions as well. This electrical approach is suitable for the heart since it is an electromechanical organ, where mechanical contractions are driven by electrical stimulus. However, there is an important limitation of the EAM system. That is, it is not able to provide an accurate anatomy. Typically, a virtual shell is used to represent the atrial wall and the vein. The points on the atrial wall, where the catheter is manually touched, are used to create this shell [15].

The catheter-based ablation process can be greatly improved if a real anatomy is used instead of the virtual shell. To ensure safe catheter maneuverability and enable delivery of effective lesions with minimal collateral damage and com-

plications, it is critical to have both the anatomical information and the electrical information available to the operator. This is particularly important for performing ablation in a complex structure such as the left atrium that is surrounded by important organs, which are vulnerable to damage if lesions are not appropriately directed with close anatomical guidance. Furthermore, even the pulmonary veins themselves are liable to be damaged with grave long-term consequences if the lesions extend deeply into the veins instead of being restricted to the ostia.

The employment of a multi-modal data integration process can provide an anatomical, physiological and functional representation. In practice, this is achieved by combining an anatomical surface model acquired by MRI/CT images and the localized electrical information measured by an EAM system. In the registration process, one obvious difficulty stems from the noise and/or outliers that are inevitably associated with the MRI/CT imaging process and the EAM data collection procedure. Unlike other organs in the body, our heart undergoes contractile motion, apart from respiratory motion, thus making it unique and very challenging to register and integrate data of different modalities. In addition to physiological variations such as changes in the heart rate, the heart rhythm and the respiratory effect, various types of heart motion are the source of outliers.

The main contribution of this work is to provide enhanced imaging of the anatomical heart surface from sparse and noisy EAM data as well as a heart shape model obtained from MRI/CT reconstruction as a prior. For 3D surface reconstruction, we adopt the level set method, which is a numerical procedure derived from the variational principle. The level set method can provide an implicit and topology free shape representation. By leveraging the 3D heart shape model, we can compensate incomplete EAM data, thereby representing the anatomical heart more accurately. The proposed method has two important advantages. First, it is robust against non-rigid deformation caused by cardiac motion and noise. Second, it can construct the optimal surface without an explicit correspondence between the MRI/CT surface and EAM data due to the implicit surface representation.

The rest of this paper is organized as follows. Previous related work is reviewed in Sec. 2. The proposed multi-modal data integration method for computer-aided ablation of atrial fibrillation is presented in Sec. 3. Both synthetic and real data are tested to demonstrate the efficiency of the proposed method in Sec. 4. Concluding remarks and future work are given in Sec. 5.

## 2 REVIEW OF RELATED WORK

Developing a computer-guided system for ablative heart surgery involves image registration or integration techniques. They are usually performed under a rigid transformation between pre-operative MRI/CT reconstruction and intra-

operative EAM data points [8, 18]. Among various registration algorithms, the Iterative Closest Point (ICP) method and its variants have been widely used for this application due to their computational efficiency [12].

The ICP algorithm begins with two meshes and an initial guess for their relative rigid-body transform. It refines the transform iteratively by generating pairs of corresponding points on the meshes and minimizing an error metric repeatedly [2]. However, the standard ICP algorithm does not take noise and outliers into account. Since noise and outliers may affect the ICP performance substantially, several ICP variants have been proposed in [20] to mitigate this problem. One popular approach to identify outliers is to use a threshold, including a certain constant, a fraction of a sorted distance and some multiple of the standard deviation of a distance [4, 13, 16]. Even with these variants, it is still challenging to deal with non-rigid deformation and differentiate inliers from outliers.

Most of previous schemes used an ICP-based method without addressing the above-mentioned problem. Instead, they focused on clinical registration. For example, Reddy *et al.* [12, 18] showed the feasibility of combining MRI with CARTO-XP in a porcine model of myocardial infarction (MI). They used the mICP (modified Iterative Closest Point) scheme for registration, but did not address the outlier problem. The modification is to adopt hierarchical registration by adding the class information in the algorithm. A clinical registration strategy that combines landmarks and surface registration was proposed in [8]. This study assessed the accuracy for each cardiac chamber using a different clinical registration method. It was observed in [10] that the size of the left atrium affects the accuracy. The patient who has a bigger chamber volume tends to have more ablation errors.

The rigid transformation assumption made by existing schemes is simple yet deficient. It often yields unsatisfactory results since a non-rigid deformation is involved between the anatomical heart model reconstructed by MRI/CT images and temporal instances of the heart at the collection of EAM data points. This physiological and anatomical variation that occurs in the formation of the heart surface model and the collection of EAM data points demands a non-rigid transformation (or equivalently diffeomorphism) between the model and the data. Woo *et al.* proposed a novel image integration technique by incorporating non-rigid deformation using level set method in [22].

To overcome the limitation of the traditional registration approach based on the rigid-transformation assumption, we formulate this problem as a 3D surface reconstruction problem from EAM data points with a given surface prior. A similar context arises in surface reconstruction from point clouds in a scanned noisy image. Surface reconstruction using an explicit representation has been considered by researchers, *e.g.*, [5, 19]. Typically, this approach needs to parameterize a large point set that could be difficult to manipulate. An-

other approach was proposed in [1, 9] to construct triangulated surfaces using Delaunay triangulations and Voronoi diagrams. It has to determine the right connection among points in the point set, which could be challenging in handling noisy and unorganized point data.

Surface reconstruction based on an implicit shape representation using the level set technique has been studied for almost two decades by applied mathematicians, *e.g.*, [6, 7, 14]. The non-parametric (or implicit) surface representation has an advantage in dealing with arbitrary topology change and deformation. Hoppe *et al.* [11] proposed an algorithm in reconstructing a surface using the signed distance function from unorganized points. Zhao *et al.* [25] proposed another algorithm using the unsigned distance function and the weighted minimal energy to reconstruct the surface. These algorithms are however restricted to situations where the population of points is dense enough to characterize the target surface. They are not applicable to our application where EAM data points are sparse and insufficient.

The problem of insufficient EAM data encountered in the 3D heart surface construction (including the left Atrium and its pulmonary veins) can be mitigated by incorporating a heart shape prior offered by MRI/CT imaging. Then, the optimal surface can be obtained by minimizing the energy functional that consists of a data fitting term and a prior knowledge term as detailed in the next section.

### 3 MULTI-MODAL DATA INTEGRATION FOR SIMULTANEOUS SURFACE RECONSTRUCTION AND REGISTRATION

In this section, we present a multi-modal data integration algorithm for simultaneous surface reconstruction and registration. This algorithm reconstructs the heart surface from measured EAM data points and a heart shape prior obtained by MRI/CT imaging using a level set method.

#### 3.1 Surface Reconstruction and Registration

Under the level set framework [21], a curve in the 2D space (or a surface in the 3D space) can be represented by the zero level set of a higher dimensional embedding function  $\phi(x)$ . That is, surface  $S(x)$  is given implicitly by

$$\begin{cases} S = \{x \in \Omega \mid \phi(x) = 0\}, \\ \text{interior}(S) = \{x \in \Omega \mid \phi(x) > 0\}, \\ \text{exterior}(S) = \{x \in \Omega \mid \phi(x) < 0\}, \end{cases} \quad (1)$$

where  $\Omega \subset \mathbb{R}^n$  and  $\phi(x) : \Omega \rightarrow \mathbb{R}$ . The shape of surface  $S(x)$  is defined by the region occupied by the union of  $S$  and its interior, denoted by  $\bar{S}$ . We can define the heaviside function  $H$  and Dirac measure  $\delta$  as

$$H(x) = \begin{cases} 1, & x \geq 0 \\ 0, & x < 0 \end{cases}, \quad \delta(x) = \frac{d}{dx}H(x). \quad (2)$$

Then, the shape of  $S$  is equal to  $\bar{S}(x) = H(\phi(x))$ . Similarly, surface  $M(x)$  for a surface model obtained from MRI/CT images can be represented implicitly via

$$\begin{cases} M = \{x \in \Omega \mid \psi(x) = 0\}, \\ \text{interior}(M) = \{x \in \Omega \mid \psi(x) > 0\}, \\ \text{exterior}(M) = \{x \in \Omega \mid \psi(x) < 0\}, \end{cases} \quad (3)$$

where  $\psi(x)$  is another embedding function and its shape is given by  $\bar{M}(x) = H(\psi(x))$ . We denote the set of measured EAM data points by

$$D = \{p_1, p_2, \dots, p_n\} \subset \mathbb{R}^3, \quad (4)$$

where  $n$  is the number of data points.

Surface  $S$  to reconstruct is likely to be close to prior surface model  $M$  and it is also attracted towards data points in  $D$ . Thus, surface  $S$  can be obtained by minimizing an energy functional that consists of a data fitting term and a prior knowledge term. Our goal is to find the embedding function  $\phi$  associated with surface  $S$  that minimizes the following cost functional:

$$E(\phi) = E_{point}(\phi, D) + \alpha E_{prior}(\phi). \quad (5)$$

#### 3.2 Derivation of Energy Terms

The energy functional in (5) consists of two terms. The first term measures how well the surface is fit to measured points based on the distance between the surface and these points. The second term measures how plausible the surface is in terms of the prior knowledge of the target surface. Parameter  $\alpha \geq 0$  is a weight that adjusts the importance of these two factors.

The data fitting term can be written as

$$E_{point}(\phi|D) = \sum_{i=1}^n \int_{\Omega} |\phi(x) \cdot \delta(x - p_i)|^2 dx, \quad (6)$$

which sums up the Euclidean distance between point  $p_i$  and  $\phi$ . Recall that  $\phi$  is a signed distance function. To impose the prior knowledge on the target surface,  $S$  should be close to prior surface model  $M$  with a smooth surface assumption. In other words, we penalize any abrupt change of the surface gradient. Here, we use two terms to represent the prior knowledge; *i.e.*,

$$E_{prior}(\phi) = E_{reg}(\phi) + E_{shape}(\phi|\psi), \quad (7)$$

where  $E_{reg}(\phi)$  is the smoothness regularization term in the form of

$$E_{reg}(\phi) = \int_{\Omega} |\nabla H(\phi(x))| dx. \quad (8)$$

and  $E_{shape}(\phi|\psi)$  is the shape dissimilarity term of the following form

$$E_{shape}(\phi|\psi) = \int_{\Omega} |H(\phi(x)) - H(\psi(T(x)))|^2 dx, \quad (9)$$

and where  $T(x)$  is a rigid transformation resulting from scaling, rotation and translation. Please note that the smoothness regularization term measures the length of the 2D curve (or the area of a 3D surface) while the shape dissimilarity term measures the symmetric difference between  $H(\phi)$  and  $H(\psi)$  under a rigid transformation.

By combining (5)-(9), we can obtain the complete energy functional  $E(\phi)$  as

$$E(\phi) = E_{point}(\phi|D) + \alpha (E_{reg}(\phi) + E_{shape}(\phi|\psi)). \quad (10)$$

Then, surface reconstruction can be formulated using the energy minimization principle as

$$\phi^* = \arg \min_{\phi} E(\phi) \quad (11)$$

under constraint  $|\nabla\phi| = 1$ , which is a property of a signed distance function. Instead of adopting the same weight  $\alpha$  for  $E_{reg}$  and  $E_{shape}$  as shown in (10), it is possible to use different weights for them.

### 3.3 Numerical Implementation

For numerical implementation, we use the following approximations for the heaviside function and the Dirac delta function [3, 24]:

$$\delta(z) = \begin{cases} 0, & \text{if } |z| > \varepsilon \\ \frac{1}{2\varepsilon} \left[ 1 + \cos\left(\frac{\pi z}{\varepsilon}\right) \right], & \text{if } |z| \leq \varepsilon \end{cases} \quad (12)$$

and

$$H(z) = \begin{cases} 1, & \text{if } z > \varepsilon \\ 0, & \text{if } z < -\varepsilon \\ \frac{1}{2} \left[ 1 + \frac{z}{\varepsilon} + \frac{1}{\pi} \sin\left(\frac{\pi z}{\varepsilon}\right) \right], & \text{if } |z| \leq \varepsilon \end{cases} \quad (13)$$

The energy functional in (11) can be minimized with respect to  $\phi(x)$  using the Euler-Lagrange equation. Finally, the gradient descent method is applied to the resultant Euler-Lagrange equation, which leads to

$$\begin{aligned} \frac{\partial \phi}{\partial t} = & -2 \sum_{i=1}^n \phi(x) \delta(x - p_i) + \alpha \left[ \delta(\phi) \operatorname{div} \left( \frac{\nabla \phi}{|\nabla \phi|} \right) \right. \\ & \left. - 2 \int_{\Omega} (H(\phi) - H(\psi)) \delta(\phi) dx \right] \end{aligned} \quad (14)$$

To solve the above partial differential equations numerically is challenging since the time step should be constrained to a small value in maintaining numerical stability. Besides, it is computationally expensive to find a high dimensional surface. Here, we employ a multi-grid scheme that adopts a hierarchical representation of the data in multiple scales and propagates the solution from the coarse scale to the fine scale to achieve computational efficiency.

### 3.4 Relationship between Variational Formulation and Bayesian Inference

This variational approach presented in Secs. 3.1 and 3.2 can be interpreted from the interpretation of Bayesian inference under a probabilistic framework. This relationship is presented in this subsection. The target surface  $S$  can be obtained by maximizing the following posterior probability:

$$P(S|D) = \frac{P(D|S)P(S)}{P(D)} \quad (15)$$

where  $P(D|S)$  is the likelihood function,  $P(S)$  is the prior probability of the surface. Maximizing this conditional probability with data points  $D$  for surface  $S$  is equivalent to minimizing its negative logarithm:

$$-\log(P(S|D)) = -\log(P(D|S)) - \log(P(S)) + c, \quad (16)$$

where  $c$  is a constant. Thus, by setting

$$E_{point}(\phi, D) = -\log(P(D|S)),$$

and

$$\alpha E_{prior}(\phi) = -\log(P(S)),$$

we can convert Eq. (16) to Eq. (5).

## 4 RESULTS AND DISCUSSION

We begin with simple yet illustrative examples to demonstrate the efficiency and robustness of the proposed algorithm. They are synthetic surfaces in the 2D space and the 3D space. Then, we will present a real patient data for further validation.

### 4.1 Synthetic data

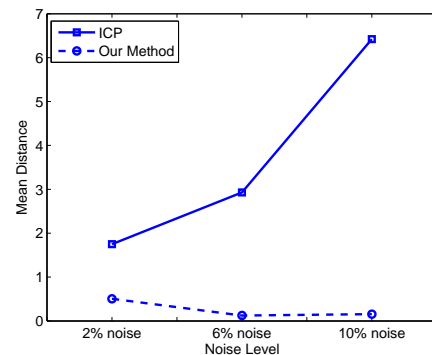


Figure 2. Comparison of mean distances between the reconstructed surface and measured data points for the 2D star example at different noise levels using ICP and the proposed algorithm.

We first compare the proposed scheme with the ICP scheme in registration accuracy using a synthetic 2D star

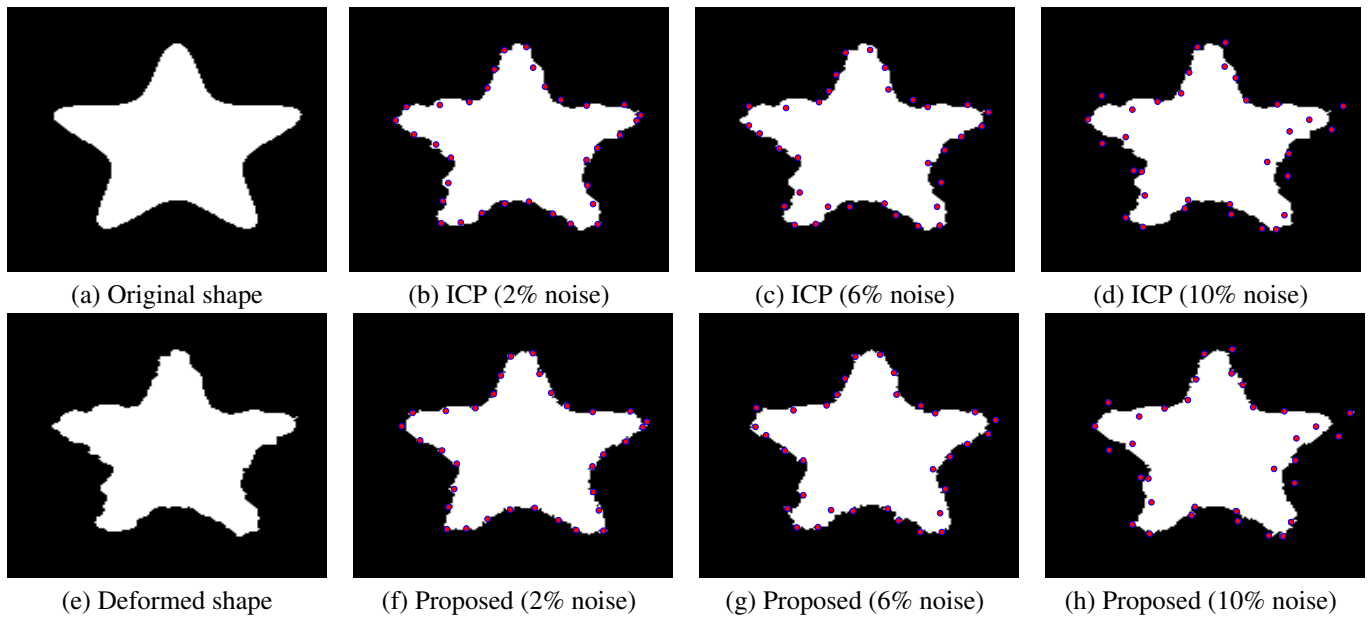


Figure 1. The shape reconstruction results for a synthetic 2D star shape, (a) the original shape, (b)-(d) ICP results using different Gaussian noise levels, (e) the deformed shape, and (f)-(h) results of the proposed method using different Gaussian noise levels.

shape as shown in Fig. 1. The original 2D star shape (image size:  $200 \times 200$  pixels) is shown in Figure 1(a). It is deformed as shown in Fig. 1(e). Furthermore, 33 noisy contour points are generated by adding Gaussian noise (2%, 6% and 10% standard deviation of contour points, respectively) to original points. Visual results of the reconstructed shape are shown in Fig. 1(b)-(d) for the ICP scheme and in Fig. 1(f)-(h) for the proposed scheme. It is clear from Fig. 2 that the proposed scheme outperforms ICP. For quantitative error analysis, we measure the mean Euclidean distance between the reconstructed surface and measured data points with varying degree of Gaussian noise. The result is shown in Fig. 2. Again, the proposed algorithm outperforms ICP significantly. This is especially true when the noise level is higher.

Next, we compare the proposed scheme with ICP using a 3D synthetic jar example. Experimental results are shown in Fig. 3, where the original and the deformed shapes are shown in (a) and (f), respectively. Points extracted from the corrupted surfaces with various Gaussian noise levels (3%, 6%, 9% and 12%) are used for visual evaluation. Reconstructed surfaces based on data points at different noise levels with ICP and the proposed algorithm are presented in Fig. 3 (b)-(e) and Fig. 3 (g)-(j), respectively. The mean distances are also measured for accuracy comparison as shown in Fig. 4. Again, the proposed algorithm is significantly better than the ICP scheme, which is especially obvious at higher noise levels, as shown in Fig. 4.

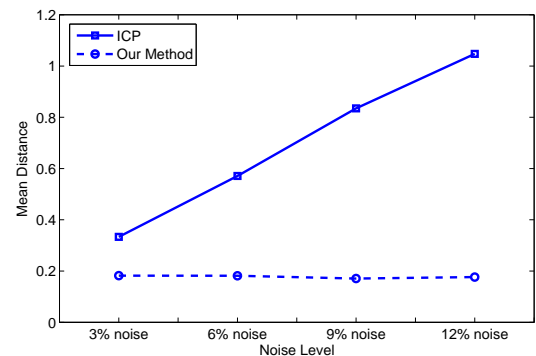


Figure 4. Comparison of mean distances between the reconstructed surface and measured data points for the 3D jar example at different noise levels using ICP and the proposed algorithm.

## 4.2 Patient data

The final example is a set of real patient data. 3D pre-operative contrast-enhanced MR angiography (MRA) was performed to delineate endocardial boundaries of the left atrium and pulmonary veins. The voxel size was  $0.78125 \times 0.78125 \times 1.5$ mm and 45 slices were used in the experiment. We obtained MRA and 250 EAM data points from the same patient. The EAM data consists of the CARTO points imported from the CARTO-XP, including measurement points as well as ablation points.

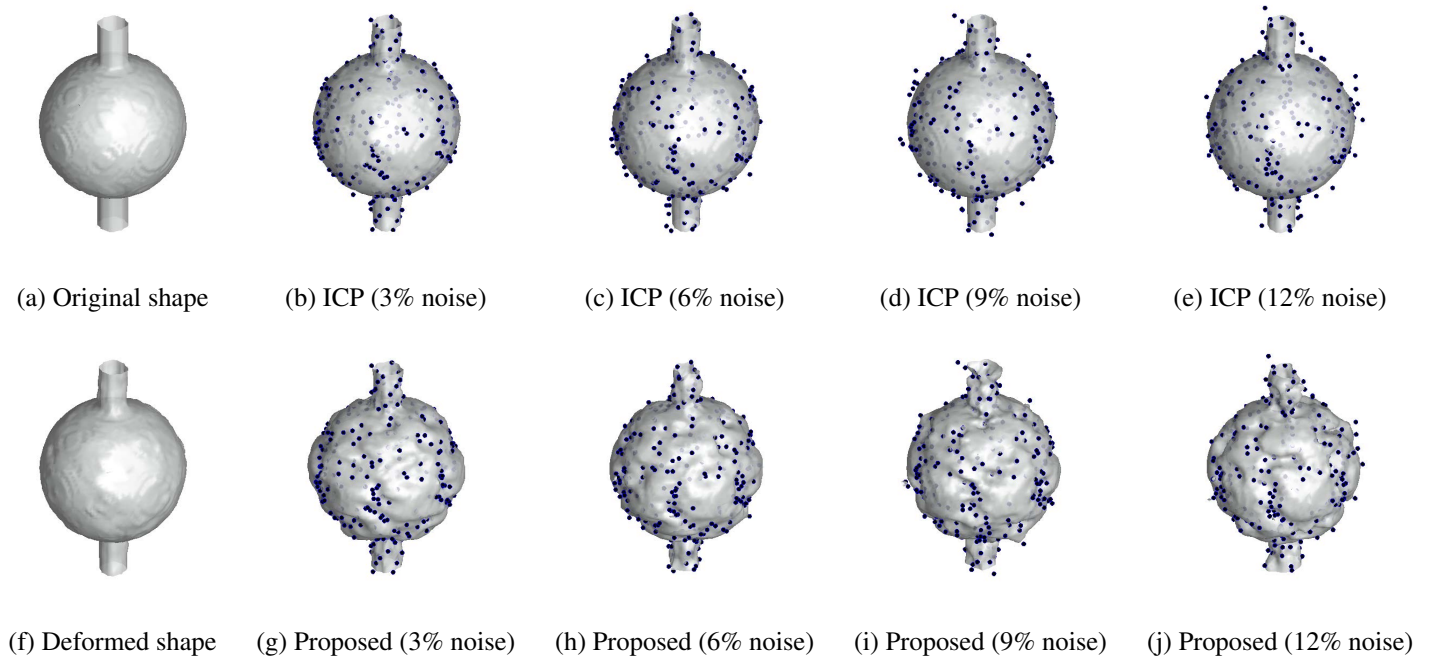


Figure 3. The shape reconstruction results for a synthetic 3D image: (a) the original shape, (b)-(e) ICP results using different Gaussian noise levels, (f) the deformed shape, and (g)-(j) results of the proposed method using different Gaussian noise levels.

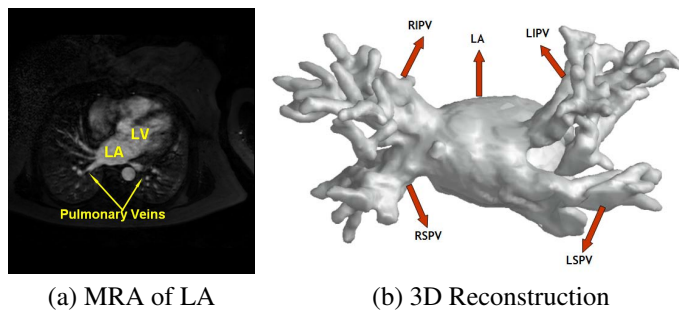


Figure 5. The 3D patient data: (a) MRA of LV and (b) 3D reconstruction result of the given MRA.

After delineating and removing unwanted regions such as the left ventricle (LV) and other small veins, we reconstruct the 3D model as shown in Fig. 5 using ITK-SNAP [23] and Matlab software. Afterwards, a two-step registration process are applied for the ICP scheme. First, we perform the landmark registration using three junctions between LA and pulmonary veins: LA-LIPV, LA-LSPV, and LA-RSPV. These points are used for the initial pose of subsequent registration. Second, surface registration using the ICP scheme is performed to refine accuracy furthermore. The resulting image is shown in Fig. 6(a).

To validate the proposed algorithm, the optimal surface is

reconstructed using 250 EAM data points by incorporating a heart shape prior from pre-operative MRA. By minimizing the energy functional, the final result is shown in Fig. 6(b), where diamonds (in blue) represent EAM data points and circles (in red) represent ablation points. Blurred points are located inside. A quantitative evaluation result can be obtained by measuring the mean distances of EAM and ablation points from the surface of the left atrium. They are reported in Table 1, which shows that the proposed approach gives better results than the ICP method.

Table 1. Performance comparison of ICP and the proposed method

	ICP	Proposed
EAM point mean distance	4.5087mm	2.4113mm
Ablation point mean distance	3.2046mm	2.0921mm

## 5 CONCLUSION AND FUTURE WORK

A novel multi-modal data integration technique using the level set method for catheter ablation of AF was presented in this paper. This technique enables reconstruction and registration simultaneously using data fidelity, regularization, and shape prior energy terms. It provides better performance than the existing ICP method in accuracy. In the proposed framework, the heart shape model from MRA reconstruction is used

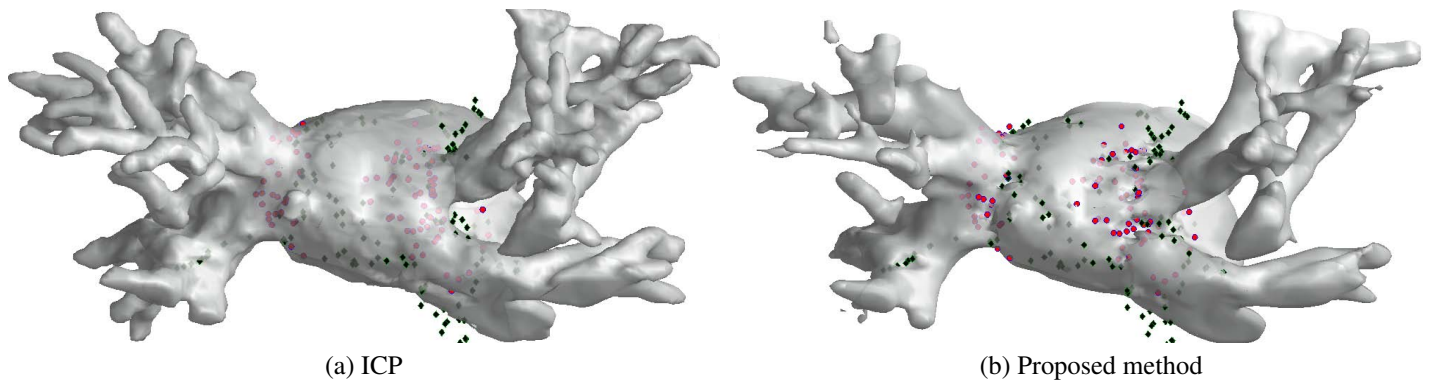


Figure 6. The surface registration results for the patient data.

as a prior shape knowledge. Thus, we can use the shape information to compensate for insufficient EAM data. Clinically, this technique can improve efficacy and safety of AF ablation by integrating EAM data and 3D imaging data.

Dynamic cardiac shape analysis will make the current integration method more precise and meaningful. We plan to incorporate a richer set of spatio-temporal shape models using dynamic shape information in the future. Besides, we may consider a localized regularization method around the point data to obtain more precise reconstruction.

## References

- [1] N. Amenta and M. Bern. Surface reconstruction by voronoi filtering. *Discrete and Computational Geometry*, 22(4):481–504, 1999.
- [2] P. J. Besl and N. D. McKay. A method for registration of 3-d shapes. *IEEE Trans. Pattern Anal. Mach. Intell.*, 14(2):239–256, 1992.
- [3] T. Chan and L. Vese. Active contours without edges. *IEEE Transactions on Image Processing*, 10(2):266–277, February 2001.
- [4] D. Chetverikov, D. Svirko, D. Stepanov, and P. Krsek. The trimmed iterative closest point algorithm. *International Conference on Pattern Recognition*, 03:30545, 2002.
- [5] C.-H. Chuang and C.-C. J. Kuo. A wavelet descriptor of planar curves: theory and applications. *IEEE Trans. on Image Processing*, 5(1):56–70, 1996.
- [6] A. Dervieux and F. Thomasset. A finite element method for the simulation of Rayleigh-Taylor instability. *Lecture Notes in Mathematics*, 771:145–159, 1979.
- [7] A. Dervieux and F. Thomasset. Multifluid incompressible flows by a finite element method. In W. Reynolds and R. MacCormack, editors, *Seventh International Conference on Numerical Methods in Fluid Dynamics*, volume 141 of *Lecture Notes in Physics*, pages 158–163, June 1980.
- [8] J. Dong, H. Calkins, S. B. Solomon, S. Lai, D. Dalal, A. Lardo, E. Brem, A. Preiss, R. D. Berger, H. Halperin, and T. Dickfeld. Integrated Electroanatomic Mapping With Three-Dimensional Computed Tomographic Images for Real-Time Guided Ablations. *Circulation*, 113(2):186–194, 2006.
- [9] H. Edelsbrunner. Shape reconstruction with delaunay complex. In *LATIN '98: Proceedings of the Third Latin American Symposium on Theoretical Informatics*, pages 119–132, London, UK, 1998. Springer-Verlag.
- [10] E. Heist, J. Chevalier, G. Holmvang, and et al. Factors affecting error in integration of electroanatomic mapping with ct and mr imaging during catheter ablation of atrial fibrillation. *Journal of Interventional Cardiac Electrophysiology*, 17(1):21–27, October 2006.
- [11] H. Hoppe, T. DeRose, T. Duchamp, J. McDonald, and W. Stuetzle. Surface reconstruction from unorganized points. *Computer Graphics*, 26(2):71–78, 1992.
- [12] Z. Malchano. Image guidance in cardiac electrophysiology. Master's thesis, Massachusetts Institute of Technology, Boston, MA, June 2006.
- [13] T. Masuda, K. Sakaue, and N. Yokoya. Registration and integration of multiple range images for 3-d model construction. In *Pattern Recognition, 1996., Proceedings of the 13th International Conference on*, pages 879–883, 1996.
- [14] S. Osher and J. Sethian. Fronts propagating with curvature dependent speed: algorithms based on the Hamilton–Jacobi formulation. *J. of Comp. Physics*, 79:12–49, 1988.
- [15] C. Pappone, S. Rosanio, G. Orte, and et al. Circumferential radiofrequency ablation of pulmonary vein ostia. *circulation*, 102:2619–2628, November 2000.
- [16] K. Pulli. Multiview registration for large data sets. In *Inlt. Conf. on 3D Digital Imaging and Modeling*, pages 160–168, 1999.
- [17] I. B. Ray and E. Heist. Treating atrial fibrillation. what is the consensus now? *Postgraduate medicine*, 118(4), October 2005.
- [18] V. Reddy, Z. Malchano, G. Holmvang, and et al. Integration of cardiac magnetic resonance imaging with three-dimensional electroanatomic mapping to guide left ventricular catheter manipulation: feasibility in a porcine model of healed myocardial infarction. *J Am Coll Cardiol*, 44(11):2202–2213, 2004.
- [19] D. Rogers. *An Introduction to NURBS: With Historic Perspective*. Morgan Kaufmann Publisher Inc., San Francisco, CA, 2001.
- [20] S. Rusinkiewicz and M. Levoy. Efficient variants of the ICP algorithm. In *Proceedings of the Third Intl. Conf. on 3D Digital Imaging and Modeling*, pages 145–152, 2001.
- [21] J. Sethian. *Level Set Methods and Fast Marching Methods: Evolving Interfaces in Computational Geometry*. Cambridge University Press, 1998.

- [22] J. Woo, B. Hong, S. Kumar, I. B. Ray, and C.-C. J. Kuo. Joint reconstruction and registration using level sets: Application to the computer-aided ablation of atrial fibrillation. In *International Conference Frontiers in the Convergence of Bioscience and Information Technologies*, Jeju, Korea, Oct 2007.
- [23] P. A. Yushkevich, J. Piven, H. Cody, S. Ho, J. C. Gee, and G. Gerig. User-guided level set segmentation of anatomical structures with ITK-SNAP. *Insight Journal*, 1, 2005. Special Issue on ISC/NA-MIC/MICCAI Workshop on Open-Source Software.
- [24] H. Zhao, T. Chan, B. Merriman, and S. Osher. A variational level set approach to multiphase motion. *J. Comput. Phys.*, 127:179–195, 1996.
- [25] H. Zhao, S. Osher, and R. Fedkiw. Fast surface reconstruction using the level set method. *1st IEEE Workshop on Variational and Level Set Methods, 8th ICCV, Vancouver*, pages 194–202, 2001.
- [26] D. P. Zipes and H. J. J. Wellens. What have we learned about cardiac arrhythmias? *Circulation*, 102(4), November 2000.